BBA - Molecular Cell Research 1868 (2021) 118911

Contents lists available at ScienceDirect

BBA - Molecular Cell Research

journal homepage: www.elsevier.com/locate/bbamcr

Menadione-induced endothelial inflammation detected by Raman spectroscopy

Ewelina Bik [a,b], Lukasz Mateuszuk [a], Marta Stojak [a], Stefan Chlopicki [a,c], Malgorzata Baranska [a,b], Katarzyna Majzner [a,b,*]

[a] Jagiellonian Centre for Experimental Therapeutics (JCET), Jagiellonian University, 14 Bobrzynskiego Str., 30-348 Krakow, Poland
[b] Faculty of Chemistry, Jagiellonian University, 2 Gronostajowa Str., 30-387 Krakow, Poland
[c] Chair of Pharmacology, Jagiellonian University, Medical College 16 Grzegorzecka Str., 31-531 Krakow, Poland

ARTICLE INFO

Keywords:
Endothelium
Oxidative stress
Mitochondria
Raman imaging
Fluorescence imaging

ABSTRACT

In this work, the effect of an early oxidative stress on human endothelial cells induced by menadione was studied using a combined methodology of label-free Raman imaging and fluorescence staining. Menadione-induced ROS-dependent endothelial inflammation in human aorta endothelial cells (HAEC) was studied with focus on changes in cytochrome, proteins, nucleic acids and lipids content and their distribution in cells. Fluorescence staining (ICAM-1, VCAM-1, vWF, LipidTox, MitoRos and DCF) was used to confirm endothelial inflammation and ROS generation. The results showed that short time, exposure to menadione did not cause their apoptosis or necrosis (Annexin V Apoptosis Detection Kit) within the 3 h timescale of measurement. On the other hand, 3 h of incubation, did result in endothelial inflammation (ICAM-1, VCAM-1, vWF) that was associated with an increased ROS formation (MitoRos and DCF) suggesting the oxidative stress-mediated inflammation. Chemometric analysis of spectral data enabled the determination of spectroscopic markers of menadione-induced oxidative stress–mediated endothelial inflammation including a decrease of the bands intensity of cytochrome (604, 750, 1128, 1315 and 1585 cm^{-1}), nucleic acids bands (785 cm^{-1}), proteins (1005 cm^{-1}) and increased intensity of lipid bands (722, 1085, 1265, 1303, 1445 and 1660 cm^{-1}), without changes in the spectroscopic signature of the cell nucleus. In conclusion, oxidative stress resulting in endothelial inflammation was featured by significant alterations in the number of biochemical changes in mitochondria and other cellular compartments detected by Raman spectroscopy. Most of these, coexisted with results from fluorescence imaging, and most importantly occurred earlier than the detection of increased ROS or markers of endothelial inflammation.

1. Introduction

Endothelial cells are involved at every stage of the development of cardiovascular diseases, and their proper function is crucial for cardiovascular system homeostasis [1]. Oxidative stress (an imbalance between antioxidants and reactive oxygen species (ROS)), promotes inflammation and endothelial dysfunction [2,3], which in turn initiates and/or accelerates the progression of various cardiovascular diseases [4]. The major source for intracellular ROS are enzymes produced by endothelium, such as NO synthesis (eNOS), nicotinamide adenine dinucleotide (NADPH) oxidases and xanthine oxidase, cyclooxygenases, lipoxygenases, and products of mitochondrial respiration [5,6]. In the vascular system, ROS not only lead to the cell damage, but also play a physiological role in controlling endothelial function and pathophysiological state. An increased ROS content is observed in cells inflammation and apoptosis, as well as in proliferation, migration, hypertension, fibrosis or angiogenesis [7–9].

Menadione (a quinone precursor for vitamin K3 synthesis [10]) is a well-known compound to induce oxidative stress, inflammation, and apoptosis in endothelial cells [3,11–13]. In vitro ROS generation may cause modifications and damage to almost all cellular chemical components, including lipid peroxidation, as well as an aggregation and denaturation of proteins. Free radicals also induce changes in DNA leading to its mutations or cytotoxic effects [14,15]. It was suggested that cytotoxicity triggered by menadione generates a production of ROS through the redox cycling – an electron from NADPH is transferred to menadione, which results in the formation of semiquinone containing free radical, and subsequent reaction with oxygen [10].

* Corresponding author at: Jagiellonian Centre for Experimental Therapeutics (JCET), Jagiellonian University, 14 Bobrzynskiego Str., 30-348 Krakow, Poland.
E-mail address: katarzyna.b.majzner@uj.edu.pl (K. Majzner).

https://doi.org/10.1016/j.bbamcr.2020.118911
Received 15 August 2020; Received in revised form 13 November 2020; Accepted 18 November 2020
Available online 21 November 2020

Raman imaging represents a useful label-free technique and is based on unique and internal spectroscopic signature reflecting biochemical cellular components. Obviously, a direct observation of ROS and oxidative stress by means of label free Raman spectroscopy is not possible, mainly because radicals are short lived and even if Raman signal from radicals would be occasionally recorded, it would be too weak and hidden in signal from cells since they. The reason is that radicals possess smaller scattering cross section than biochemical components of the cells. An alternative would be Raman spectroscopy with the use of chemosensors (molecular and nanoscaled probes) dedicated for detection of ROS in cells or ultra-fast Raman approaches [16]. However it can be investigated indirectly by analyzing the effects of ROS on cellular biochemistry (proteins, nucleic acids and lipids). Oxidative stress causes relatively strong biochemical changes at the subcellular level. This technique can detect ROS-induced alterations in cellular biochemical content. Furthermore, an imaging of a single cell with micrometric resolution should provide information not only about biochemical alterations resulting from the active action of ROS, but also about the subcellular localization of these changes. Raman spectroscopic techniques have already been applied to probe, for example, oxidatively induced mitochondrial dysfunction in living cells [17] or changes in mice skeletal muscles [18] and vascular inflammation [19]. In the previous work concerning a detection of nanoparticles induced oxidative stress by means of Raman spectroscopy, an alterations in intensities of doublet Raman bands around 785 (nuleic acids) and 810 cm^{-1} (RNA) in the cytoplasm area was indicated as the spectroscopic markers of oxidative stress [20]. Authors have shown that different cellular responses and mechanisms leading to cell death between cancerous and non-cancerous cell lines can be differentiated by using the spectral markers of the cellular toxic events. The Raman bands at 785 and 810 cm^{-1}, were identified as a signature of ROS related changes in the biochemical composition of the cell upon a toxicant exposure [20]. The final effects of acute oxidative stress may lead to a cell death by apoptosis and necrosis – both processes could be detected by Raman spectroscopy [21]. However, Raman spectroscopy has not been widely used as yet to detect cellular oxidative stress.

This paper evaluates the biochemical alterations in human aorta endothelial cells (HAEC) caused by ROS-dependent inflammation induced by menadione. We applied the complex approach including fluorescence and Raman imaging with two excitation wavelengths (532 and 488 nm) in order to analysis in detail this in vitro endothelial model of pharmacologically induced oxidative stress.

2. Materials and methods

2.1. Cell culture

Human aortic endothelial cells (HAEC; Lonza) were maintained in supplemented endothelial growth media (EGM-2MV, Lonza) at 37 °C/ 5% CO_2. Cells were regularly tested for Mycoplasma contamination using the MycoAlert Mycoplasma DetectionKit (Lonza). HAEC at 2nd or 3rd passage were seeded at a concentration of 18×10^4 and rested for 24 h on calcium fluoride windows (CaF_2, 25 × 2 mm, Crystran LTD) for Raman measurements, 6-well plate for flow cytometry and 96-well plate for fluorescence imaging. HAEC were treated with 0.1–70 μM menadione sodium bisulfate (menadione, Sigma Aldrich) for 1, 3, 6, 24 h.

2.2. Raman measurements with data analysis and processing

Raman images were acquired using a confocal Raman microscope (WITec alpha300, Ulm, Germany) supplied with air-cooled solid-state lasers operating at 488 and 532 nm, coupled to the microscope through an optical fiber. The scattered light was directed to the spectrometer using a 50 μm core diameter multimode fiber. A water immersion objective (60×/1.0 NA) was applied, and the power of the laser measured in the air just after the objective was ca. 30 mW. Data were collected with the acquisition time per spectrum of 0.5 s, sampling density of 2 μm and the spectral resolution of 3 cm^{-1}.

Recorded spectra were pre-processed according to the standard protocol [22] - which includes cosmic spike removal and background subtraction (polynomial 3rd order, separately adjusted into two spectral windows – fingerprint and high wavenumber range for spectra obtained with 488 and 532 nm lase lines. Next, cluster analysis (CA; k-means, KMC; Manhattan distance) was performed with WITec Project Five 5.1 software. CA enabled to define major and spectroscopically characteristic area of the cell (nucleus, lipid rich cytoplasmic area with strong contribution of endoplasmic reticulum and protein-rich cytoplasmic area). CA provides cluster maps and average spectra of defined classes, which were further analyzed to provide information about the biochemical changes between healthy and menadione-treated cells. The further processing of spectral data was executed using OPUS (version 7.0, Bruker Optic, Ettingen, Germany) and Unscrambler X (version 10.3, Camo Software, Oslo, Norway) software packages.

2.3. Fluorescence microscopy and image analysis

After incubation with menadione, cells were washed in PBS solution and fixed with 4% buffered formalin for 10 min at room temperature. Labeling procedure was started immediately after treatment. Before staining HAEC were permeabilized with Triton X-100 (1:1000). Subsequently cells were washed and blocked for 15 min with 5% normal goat serum (Jackson Immuno Research, Cambridgeshire, UK). HAEC were incubated overnight with primary antibodies using rabbit-anti-mouse von Willebrand factor (Abcam, Cambridge, UK; 1:100), mouse anti-ICAM-1 (ThermoFisher, Waltham, MA,USA; 1:250) and rat anti-VCAM-1 (ThermoFisher, Waltham, MA,USA; 1:200) in 4 °C. Next, cells were washed and probed with secondary antibodies Alexa Fluor 488 goat-anti-rabbit, Cy3 goat-anti-rat, Biot SP-conjugated goat-antirat and Alexa Fluor 594 streptavidin (Jackson Immuno Research, Cambridgeshire, UK; 1:300), respectively. Lipids were visualized by LipidTOX Deep Red staining (Invitrogen, Carlsbad, CA, USA; 1:200), and cell nuclei were counterstained by Hoechst 33342 (Invitrogen, Carlsbad, CA, USA; 1:1000).

Images were acquired using 20× magnification objective on CQ1 Confocal Quantitative Image Cytometer (Yokogawa, Tokio, Japan). The images analyses were carried out using Columbus 2.4.2 Software (Perkin Elmer, Waltham, MS, USA).

2.4. ROS detection

For measurement of ROS, 2′,7′-dichlorodihydrofluorescein diacetate (H2DCFDA, DCF) and MitoTracker™ Orange CM-H_2TMRos (MitoRos) from Invitrogen, were applied. In DCF acetate groups are cleaved by oxidation changing nonfluorescent form of probe to fluorescent one [23]. MitoRos is reduced version of MitoTracker which stains mitochondria. However, MitoRos stains mitochondria well, only upon oxidation conditions [24]. Cells were loaded with 10 μM of a DCF probe in HBSS solution and incubated at 37 °C for 30 min. Then cells were washed and immediately measured by plate reader (BioTek). On separate plate, cells were immersed in HBSS solution and labeled with 500 nM of a MitoRos and Hoechst 33342 (1:2000) simultaneously and were incubated at 37 °C for 30 min, then washed and measured immediately by CQ1 Confocal Quantitative Image Cytometer.

2.5. Flow cytometry

To detect apoptotic and necrotic cells after 3 h exposure to menadione, cells were labeled fluorescently with FITC Annexin V Apoptosis Detection Kit I, according to the manufacturer's instruction (BD Biosciences, Franklin Lakes, NJ, USA). Briefly, HAEC cells were harvested by Accutase solution (Sigma-Aldrich), washed twice with PBS and resuspended in 100 μl of binding buffer. Then, 5 μl of annexin V-FITC

and 5 μl of PI staining solution were added to the cell suspension and cells were incubated in the dark for 15 min, at room temperature. Following the incubation, 400 μl of binding buffer was added to each tube. The labeled cells were immediately measured using a BD LSR II flow cytometer. The frequency of viable cells, early apoptotic cells, late apoptotic and necrotic cells, were determined using BD FACSDiva software. The data were determined by three independent experiments.

2.6. MTT assay

For MTT test cells were grown in 96-well plates. After 24 h of incubation, with or without menadione, to each well containing 200 μl of media, 20 μl of 5 mg/ml 3-(4,5-dimethyl-2-thiazolyl)-2,5-diphenyl-2H-tetrazolium bromide (MTT, PanReac AppliChem) were added immediately. Cells were incubated for the next 1.5 h at 37 °C and afterwards, media was removed and plates were frozen at −20 °C for next 24 h. In the further step isopropanol was added to each well and the plate was placed on a plate shaker for 15 min to dissolve a dye. The absorbance of such prepared samples was measured at 570 and 650 nm by a Synergy 4 plate reader (Biotek, VT, USA).

2.7. UV–Vis - data collection and analysis

Absorption spectra (UV–Vis) of cytochrome *c* standard solutions at 0.025–0.4 μM concentration were recorded on a Perkin Elmer double beam spectrophotometer Lambda 950 in the range of 250 to 600 nm in a cuvette of 1 mm path length (results presented in Fig. SM1).

2.8. Statistical analysis

Statistical analyses were performed using OriginPro 2018 software. All data are presented as mean ± standard deviation. Statistical significance was calculated using one-way analysis of variance (ANOVA) with post-hoc Tukey's test. Statistical significance was defined as at least $p < 0.05$.

3. Results

3.1. Characterization of menadione-induced endothelial response

As shown in Fig. 1A (Hoescht) and Fig. 1G (MTT), menadione decreases the viability of HAEC line (Fig. 1A) in concentration- and time-dependent manner as evidenced by MTT assay and counting of Hoechst–stained cells. Menadione did not noticeably affect endothelial cells viability up to the concentration of 50 μM after 3 h of incubation, but after 6 and 24 h of a menadione treatment clearly affected cellular viability is seen at a concentration of 10 μM or higher (Fig. 1A, G).

Short-term (3 h) endothelial cell response to the menadione at the concentration in the range of 10–30 μM did not result in any appreciable toxicity to endothelium in the short term as confirmed by flow cytometry–based assessment of necrosis or apoptosis (1F) within the 3 h timescale of measurement. However, short-term (3 h) endothelial cells response to menadione was featured by an inflammation as evidenced by increased expression of intercellular adhesive (ICAM-1), vascular cell adhesion (VCAM-1) and von Willebrand factor (vWF) (Fig. 1B–D). Simultaneously, increased number of lipid spots in the cytoplasm was detected by LipidTox staining (Fig. 1E). It is worth to highlight that 1 h of incubation did not result in noticeable endothelial inflammation (results presented in Fig. SM2).

To confirm that menadione-induced endothelial inflammation was linked to ROS generation, DCFDA dye and MitoRos were used. As shown in Fig. 2, DCF and MitoRos-based fluorescence significantly increased after 3 h incubation with menadione at a concentration of 30 or 50 μM, but this effect was not seen for lower concentrations of menadione (1, 10 μM). Shorter incubation time of endothelial cell with menadione (1 h) was not associated with ROS generation (Fig. 2). Altogether, these results show that short-term incubation with menadione (30–50 μM) resulted in ROS-dependent endothelial inflammation, but not in in any appreciable endothelial toxicity and this model was used for the further studies.

3.2. Raman imaging of live HAECs exposed to menadione

For all recorded Raman images k-means cluster analysis (KMC) was applied, as described in [25–27], to obtain the average spectra of selected cell areas: nucleus, cytoplasm and endoplasmic reticulum-rich one (ER). Briefly, the main spectral features attributed to specific cell regions, were the high intensities of: nucleic acids marker bands at 785 and 1092 cm^{-1} (nucleus area), cytochrome bands at ca. 751, 1128, 1315 and 1585 cm^{-1}, and phospholipid band, e.g. at 720 cm^{-1} (assigned to mitochondria and phospholipid membranes in ER region). Within cytoplasm region, Raman signal for cytochrome, phospholipids and overall is rather low and reflects rather protein-rich content.

In Fig. 3A ER spectra of the control and menadione-treated cells illustrate the most evident changes induced by menadione, i.e. a decrease in the intensity of the cytochrome marker bands at 604, 751, 1128, 1315 and 1585 cm^{-1}. Even though, some of these bands overlap with Raman signals from lipids and proteins (1128, 1315 cm^{-1}), the change in the intensity most probably comes from cytochrome bands. The observed decrease of 1005 (Phe ring breathing mode [28]) and 1175 cm^{-1} (C—H in-plane bending vibrations in Phe and Tyr [29]) bands after 1 or 3 h indicated changes in a protein content in ER area. Moreover, a decrease in 1336 cm^{-1} band after 1 h was remarked. All aforementioned changes became more evident after 3 h incubation, in comparison to 1 h of incubation. The 1445 cm^{-1} band assigned to scissoring CH_2/CH_3 vibrations in lipids, increased in intensity, which was a premise for the rise in lipid content in the ER-rich area and suggested slight changes in unsaturation ratio of lipid profile in comparison to control. This observation is in a good agreement with previously reported results indicating that inflammation is manifested in Raman spectra of endothelial cells by changes in the lipid profile of and the presence of lipid droplets in perinuclear area [30].

In Fig. 3B an average value of integral intensity for marker bands of proteins (Phe), nucleic acids and cytochrome are presented to illustrate clearly changes in the intensity of discussed bands, despite possible disruptions by resonance background of cytochrome (related to the fluorescence), and hence, its nonlinear dependence on concentration [31]. The decrease in cytochrome bands upon exposure to menadione, and therefore to oxidative stress, is associated with its oxidation, but not with changes in its distribution or concentration, similarly to [17]. The integration of selected bands indicated their decrease in the intensity (785 and 1005 cm^{-1} bands associated with nucleic acids and phenylalanine (Phe), respectively), just after 1 h of incubation with menadione. According to variance analysis results, changes of integral value for Phe and cytochrome signal after 1 h were statistically significant and after 3 h of incubation this direction of changes was even deeper (ANOVA, $p < 0.01$).

Raman imaging with 488 nm line gave the spectra of cells free of the dominating cytochrome bands due to resonance effect, hence the effect of oxidative stress on protein-lipid content was exposed. Fig. 4 compares the averaged spectra extracted from ER-rich area of control and menadione-treated cells and clearly illustrates an increase in the intensity of: phospholipids bands at 722 cm^{-1} (attributed to the symmetric stretching vibrations of the choline ($N^+(CH_3)_3$ group [32]) and 1085 cm^{-1} (phosphodioxy groups [33]), carbon-carbon single bond vibrations at 1303 and 1445 cm^{-1} (CH_2 twisting and scissoring modes, respectively [32]), and markers of double bond at ca. 1265 and 1660 cm^{-1} (due to C═C stretching and ═CH deformation vibration, respectively [32])). After 3 h of incubation, the spectral profile of the ER was much more lipidic in comparison to the control cells. Narrowing of 1265 and 1305 cm^{-1} bands together with an increase in their intensity reflected a higher cellular lipid content for incubated cells. Additionally,

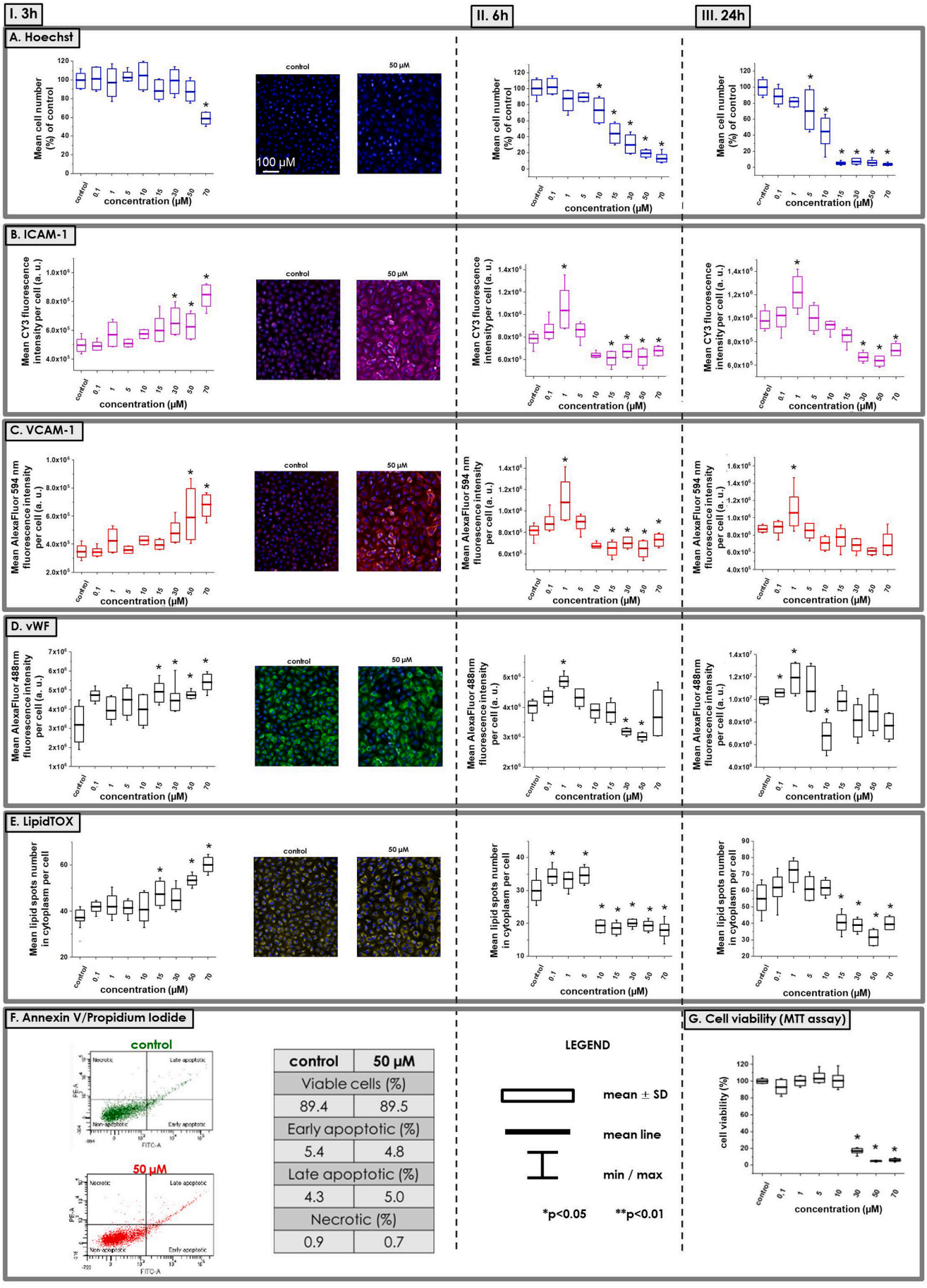

control	50 µM
Viable cells (%)	
89.4	89.5
Early apoptotic (%)	
5.4	4.8
Late apoptotic (%)	
4.3	5.0
Necrotic (%)	
0.9	0.7

(caption on next page)

Fig. 1. Response of HAEC cells to menadione after 3, 6, 24 h of incubation: (A) Number of cells calculated based on Hoechst staining (% of control). Inflammatory response to menadione was evaluated based on (B) ICAM-1, (C) VCAM-1, and (D) vWF expression together with (E) the amount of lipid spots in the cytoplasm. (F) Detection of apoptosis and necrosis of cells after 3 h of incubation with menadione were evaluated with Annexin V-FITC Apoptosis Detection Kit and analyzed by flow cytometry; (G) Cell viability based on MTT assay after 24 h incubation with menadione.

Raman bands that appeared at around 425 and 705 cm^{-1} were implying the presence of traces of cholesterol esters [34]. Such an observation, along with the increased intensity of bands at 1265, 1303, and the ratio of bands 1445/1660, indicates significant alterations in lipid profile of cells upon oxidative stress. Moreover, a signal at 1005 cm^{-1} (Phe) has also decreased.

To confirm and support changes observed directly in the Raman spectra, a Principal Component Analysis (PCA) was performed on the average spectra of the ER region of single cells. The results (Fig. 5) confirmed all differences discussed. Generally, PCA revealed a decrease in the intensity of cytochrome band (608, 750, 1128 and 1312 cm^{-1}), when spectra were recorded with 532 nm excitation and indicated a higher content of lipids (705, 811, 1256, 1309 and 1445 cm^{-1}) for menadione-treated cells, when cells were measured with 488 nm laser. In the spectra of pure menadione (both solid state and solution; Fig. SM4) the most prominent Raman bands are 487 cm^{-1} (ρC-C), 1006 cm^{-1} (νC-C), 1042 cm^{-1} (ring νC-C), 1607 cm^{-1} (νC=C) and 1695 cm^{-1} (νC=O) in quinone moiety, respectively [35–37]. PCA analyses for control and menadione-treated cells were done in the 500–1500 cm^{-1} spectral window (Fig. 5) and only two bands (1006 and 1042 cm^{-1}) can be observed in this range, but it should be noticed that in cells those bands are characteristic for phenylalanine and are markers of proteins and glutaraldehyde-fixation. However, if menadione had accumulated in cells or binds to cellular components, those bands would be prominent in spectra and positive loadings for menadione treated cells rather than for cells, while in Fig. 5B they are observed for control group indicating higher protein content for this group of cells.

Fig. 6 demonstrates further noticeable differences in the Raman profiles of treated and non-treated cells, within the cytoplasm region. But, despite similarities to ER, cytoplasm spectra had lower signal-to-noise ratio, which made them less reliable. What is more, Fig. SM3 illustrates no differences in the intensity of the 785 cm^{-1} band in the spectra taken from nucleus. The slight changes were observed only at the level of spectral noise and could not be considered as markers what indicates that applied time of incubation does not result in oxidative damage of this cellular structure. In addition, a decrease in intensity of nucleic marker band in ER area could possibly reflect mitochondrial DNA damage by ROS.

3.3. Raman imaging of glutaraldehyde fixed HAECs exposed on 50 μM menadione for 3 h

In order to check applicability of described markers for proposed oxidative stress model, next experiment based on fixed cells was performed also on HAEC cells after 3 h exposure to 50 μM menadione. Cells were fixed for 5 min with 2.5% glutaraldehyde and measured with 532 nm laser. Glutaraldehyde fixation considerably influenced Raman spectra what is observed by a decrease of intensity of the cytochrome bands. Additionally, 1039 cm^{-1} band was the main one that differentiated spectra from live cells vs. the fixed ones, as described elsewhere [38]. Its occurrence was an effect of proteins–glutaraldehyde cross-linking reaction and changes in the Phe conformation [39]. Fig. 7 illustrates that the most of changes noticeable for live cells can be also noticed for the fixed cells. Differences between those two approaches were observed in the contrast of Raman signal and decreased resonance background of cytochrome, which had a big impact on the Raman bands intensities.

Fig. 7 manifests the most prominent alterations after incubation in ER spectra: the cytochrome bands (751, 1128, 1315, 1585 cm^{-1}) and phenylalanine-tyrosine (1175 cm^{-1}) have decreased in their intensity, when both phenylalanine (1005 cm^{-1}) and nucleic acid (785 cm^{-1}) bands only slightly changed, whereas Raman features for lipids (718, 1085, 1145 cm^{-1}) showed an increase in the intensity for menadione-treated cells. PCA confirmed that changes in cytochrome signal were consistent and observed both for live and fixed cells. Raman spectra of glutaraldehyde fixed cells resulted in a decreased signal of cytochrome upon its oxidation [38], but application of the same cells treatment (for the control and menadione-treated group) provided an independent comparison of changes in the analyzed model. Fixation of cells enabled us to measure a higher number of cells with no biochemical changes which could be linked to apoptosis.

4. Discussion

Results obtained from fluorescence staining showed that 3 h exposure on menadione resulted in noticeable oxidative stress-mediated inflammation (increased expression of ICAM-1, VCAM-1, vWF, LipidTox and ROS), and it did not cause apoptosis or necrosis in endothelial cells (Annexin V Apoptosis Detection Kit) within the 3 hour timescale of

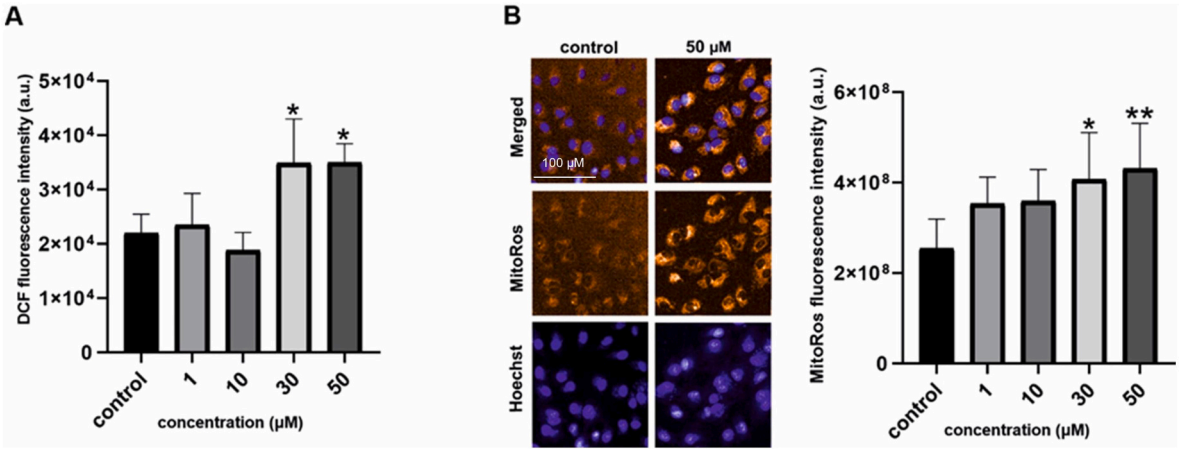

Fig. 2. ROS production evaluated by the average DCF-mediated fluorescence intensity (A) and the average MitoRos fluorescence (B), after 3 h exposure of HAECs to 1, 10, 30, 50 μM menadione concentrations.

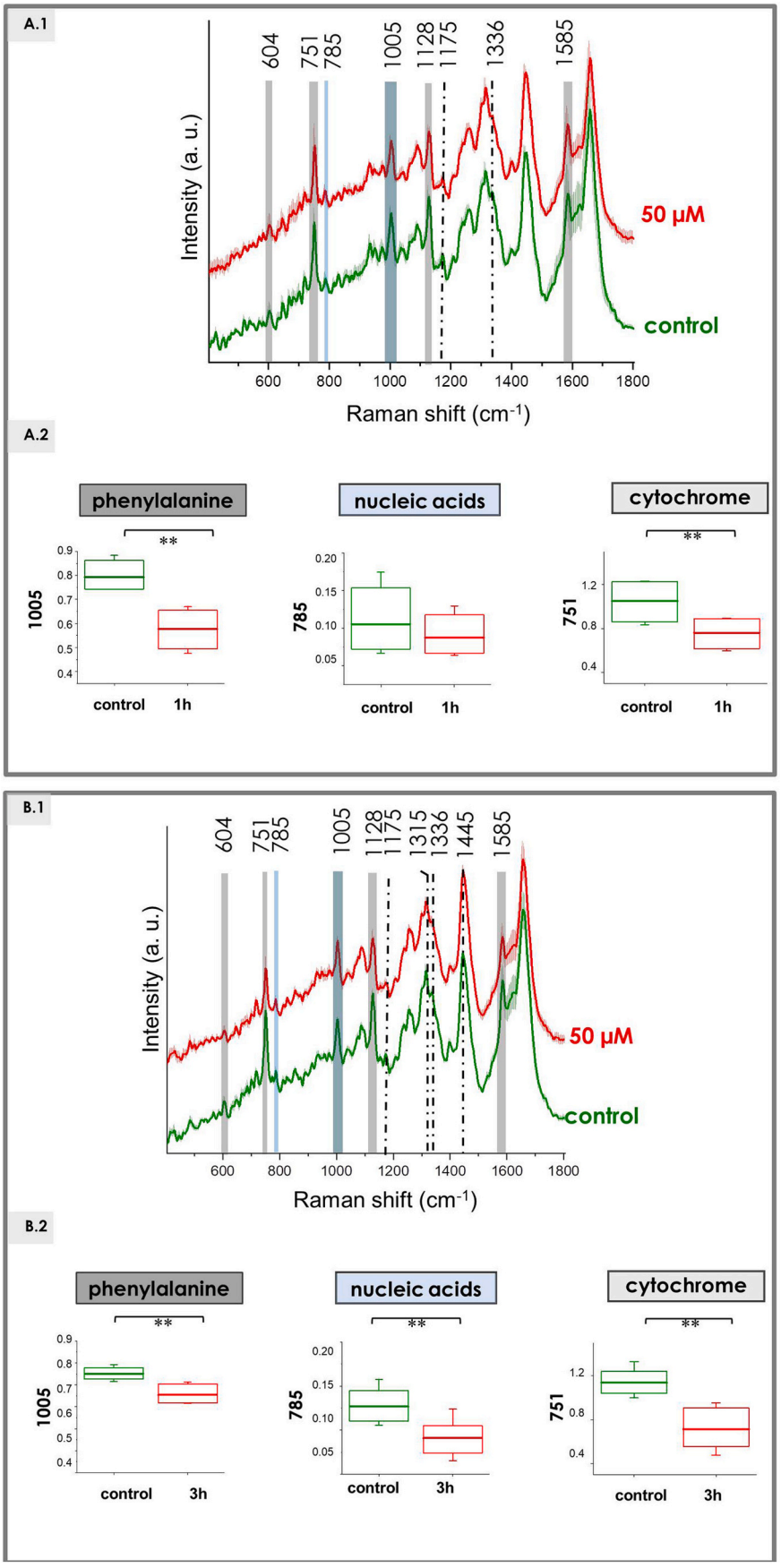

Fig. 3. Average ER spectra (with SD) for HAEC: control (green) & exposed on 50 µM menadione (red) for 1 h (A.1) and 3 h (B.1), obtained with 532 nm laser line. Integral intensities of phenylalanine (1005 cm^{-1}), nucleic acids (785 cm^{-1}), cytochrome (751 cm^{-1}), after 1 h (A.1) and 3 h (B.1).

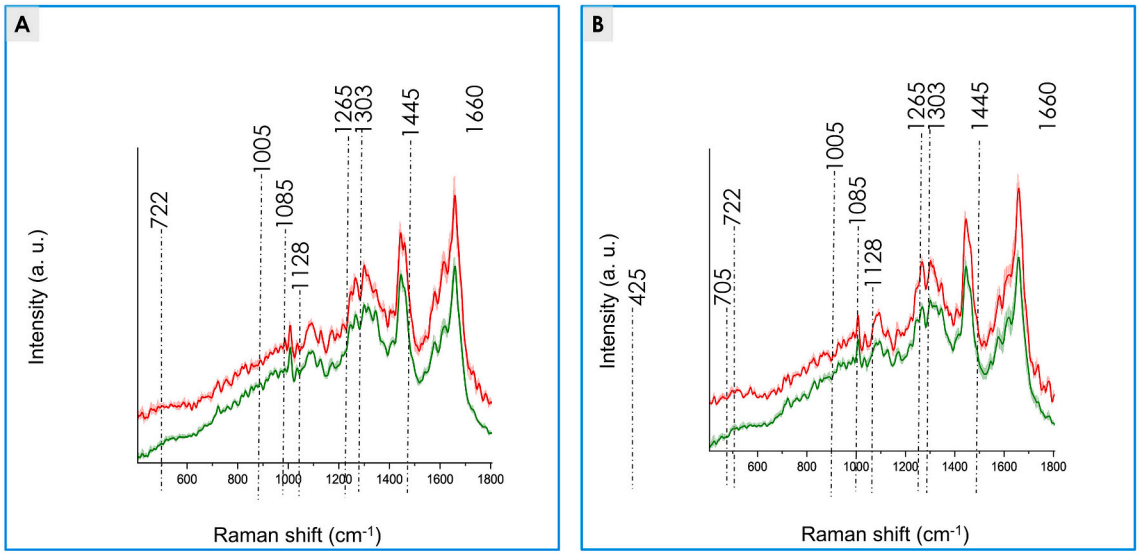

Fig. 4. Average ER spectra (with SD) for HAEC: control (green) & exposed on 50 μM menadione (red) for 1 h (A) and 3 h (B), obtained with 488 nm laser line.

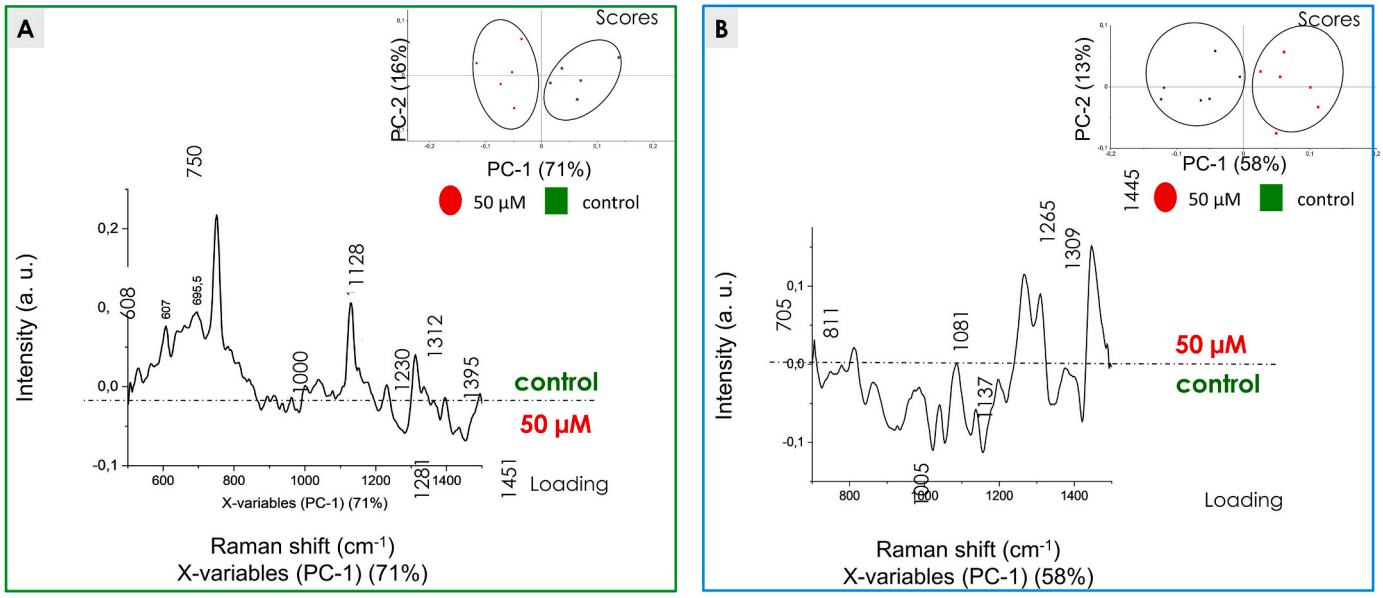

Fig. 5. PCA results for the spectra of ER area from control & cells exposed for 3 h to 50 μM menadione, measured with (A) 532 nm and (B) 488 nm excitation.

measurement.

Therefore, the biochemical changes revealed that oxidative stress-mediated inflammation is linked to the panel of spectroscopic markers of early oxidative stress-mediated inflammation in endothelial cells. As mentioned in the previous studies, the application of 532 nm laser line provided the characteristic signature for cytochrome (mitochondrial heme-containing protein) [40], due to its resonance Raman effect [17,41]. In turn, the excitation at 488 nm complements the spectroscopic characteristic of cells with detailed insight into lipids or proteins alterations.

The main observation from Raman spectra obtained with 532 nm laser was the decrease of cytochrome bands. This hemeprotein, found in mitochondria, absorbs visible light at around 530 nm (Q band in UV–Vis spectrum) (Fig. SM1). Thus, when exciting cells with a 532 nm laser, intense bands from cytochrome *c* and/or *b* were observed in Raman spectra, directly related to the resonant signal. It is highly possible that observed decrease of cytochrome marker bands intensities (751, 1130, 1315 and 1585 cm^{-1}) reflected the cytochrome oxidation state due to the excessive amount of ROS. The reduced form of cytochrome manifested itself by Raman marker features mentioned above. Furthermore, resonance Raman spectra of pure cytochrome in a certain range of concentrations exhibit signal intensity-concentration dependence and allow the concentration of cytochrome to be determined. Moreover, we investigated the resonance Raman spectra of pure cytochrome *c* in solution at 0.2 μM concentration after 5 min incubation with H_2O_2 (0.1–0.8 μM) in order to measure a reference level of cytochrome oxidative damage. As expected, the incubation of cytochrome *c* solution with H_2O_2 caused a decrease in the intensity of its bands on Raman spectra. This basic model imitates the oxidative pathways in vitro and, despite some limitations, confirms a final conclusion for cytochrome changes observed in response to menadione in HAECs.

In vitro oxidative stress alters the structure and composition of proteins, nucleic acids and lipids, which was reflected by several differences between the spectra collected from the control and menadione-incubated cells. In ER-rich cellular area the decrease in the nucleic acid band was observed, suggesting the damage of mitochondrial DNA.

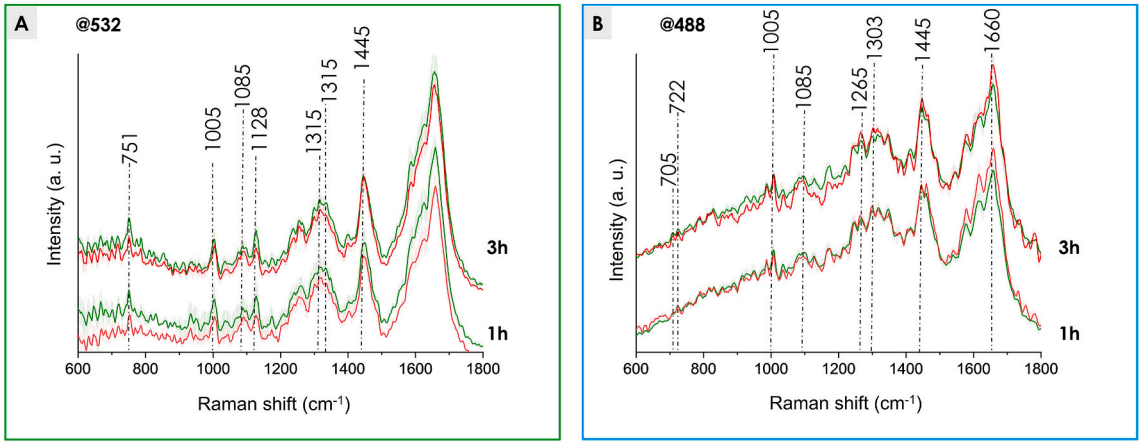

Fig. 6. Average spectra of cytoplasm (with SD) for HAEC: control (green) & exposed on 50 μM menadione (red) for 1 h and 3 h, obtained with 532 nm (A) and 488 nm (B) laser line.

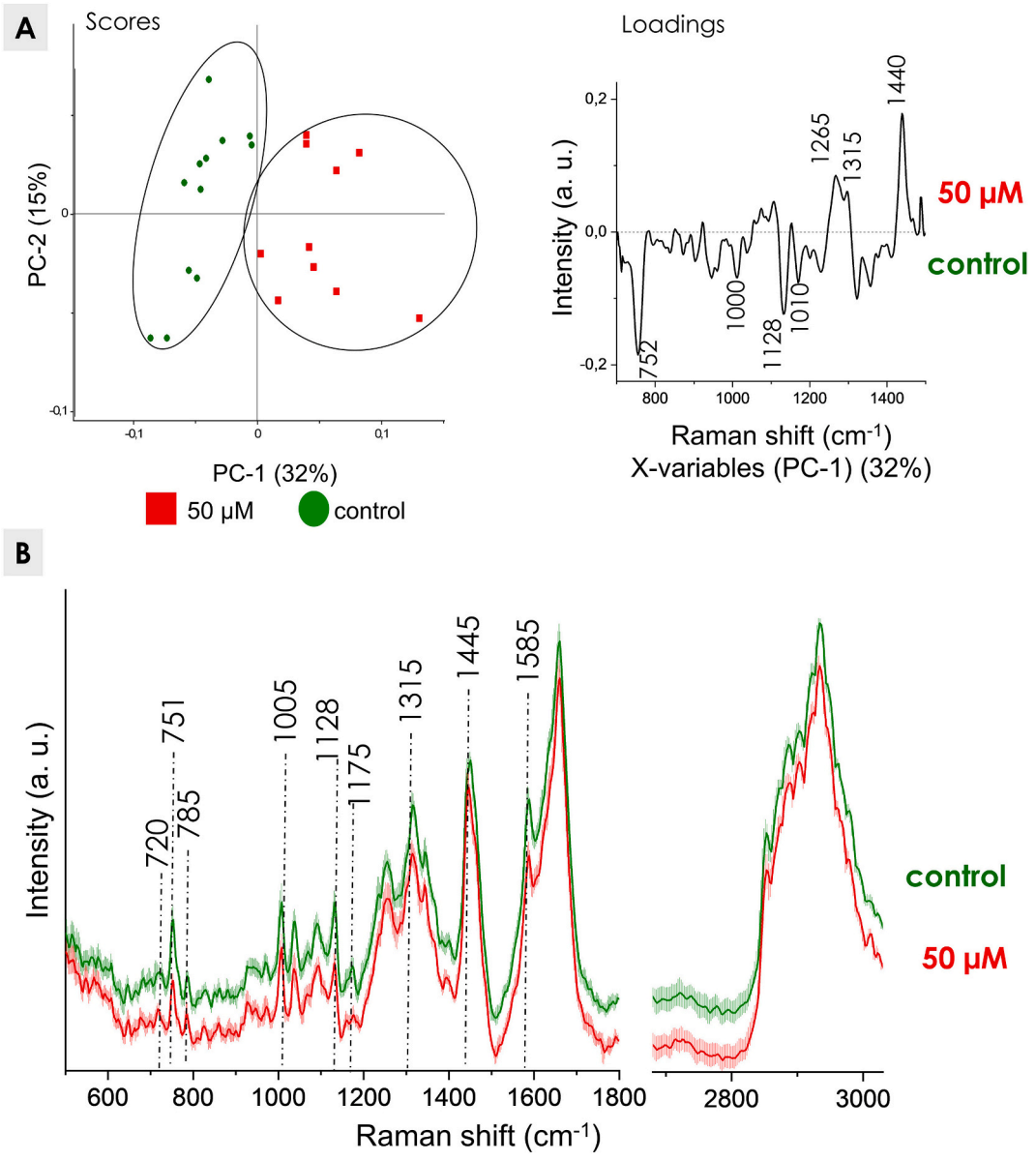

Fig. 7. (A) PCA of the spectra of ER area from fixed control & cells exposed to 50 μM menadione for 3 h, measured with 532 nm. (B) Average ER spectra (with SD) for fixed HAEC: control (green) & exposed on 50 μM menadione (red) for 3 h, obtained with 532 nm laser line.

Nuclear areas after short-term (3 h) incubation were not characterized by spectra alterations, which suggested the lack of apoptosis activation and unaffected structure of the nucleus. Measurements carried out with 488 nm laser line demonstrated changes in spectral features originating from lipids and proteins. The higher content of lipids was concluded from increased intensities of lipid marker bands (722, 986, 1081, 1265, 1309, 1445 cm^{-1}). This observation was consistent with LipidTox fluorescence staining, where an increased number of lipid spot was detected, what could be considered as a marker of inflammation induced by oxidative stress. Even though, phosphatidylserine externalization is a well-known marker of apoptosis, the change in the phospholipid band at around 720 cm^{-1} should not be considered as its unambiguous marker. By comparing the Raman spectra of various pure phospholipid compounds, a band around 720 cm^{-1} can be seen only for phosphatidylcholine [42]. Changes related with the increased unsaturation level of ER lipids for menadione-treated cells may be related to an increased production of eicosanoids and inflammation mediators. Altogether, these observations indicated an increased content of carbonyl-based biochemical compounds (such as lipids and phospholipids) within the cells after the exposure to menadione. In turn, a decrease in the intensity of the 1005 cm^{-1} (Phe) band, may suggest an oxidative damage of proteins. Raman changes observed for live cells were also successfully verified on fixed cells with 532 nm laser. Apart from the decrease in the intensity of cytochrome bands, also changes in lipids (similar to 488 nm laser line) were observed. This observation confirms that Raman spectroscopy can be used for detection of subtle biochemical changes due to oxidative stress even for the fixed cells. The Raman imaging measurement is time-consuming if a high spatial resolution is applied, therefore work with a fixed material is preferable.

5. Conclusions

A comprehensive spectroscopic assessment of biochemical alterations in endothelial cells triggered by menadione-induced oxidative stress was performed. We demonstrated a panel of Raman markers characteristic for an early oxidative stress-induced endothelial inflammation in response to menadione, e.g. a decreased intensity of cytochrome, nucleic acids and Phe-specific bands together with increased lipid content and their higher unsaturation. Alterations in lipid contents included also changes in cholesterol esters (425 and 705 cm^{-1}) and phospholipids (722 cm^{-1}) bands.

In conclusion, menadione-induced endothelial oxidative stress resulting in endothelial inflammation is featured by significant alterations in number of biochemical changes in mitochondria and other cellular compartments detected by Raman spectroscopy. Importantly most of these features not only coexisted with, but also occurred before the detection of increased ROS or biomarkers of endothelial inflammation by fluorescence spectroscopy. Thus, changes in Raman spectra may be regarded as early features of menadione-induced endothelial inflammation and their comparison to the well-established fluorescence approach indicated the advantage of Raman-spectroscopy-based methodology for early and complex detection of changes in lipids, proteins, cytochrome and nucleic acids.

Supplementary data to this article can be found online at https://doi.org/10.1016/j.bbamcr.2020.118911.

CRediT authorship contribution statement

SC, KM, EB, MB – Conceptualization, SC, KM, MB - Supervision; EB - Writing - original draft and Visualization; KM, SC – Resources and Project administration; EB, LM, KM and MS - Investigation, Methodology; EB, KM - Formal analysis, Writing - review & editing; KM - Funding acquisition. All the authors reviewed and accepted the final version of the manuscript.

Declaration of competing interest

The authors declare that they have no known competing financial interests or personal relationships that could have appeared to influence the work reported in this paper.

Acknowledgements

This work was financed by the Polish Ministry of Science and Higher Education (Iuventus Plus, project number 0464/IP1/2016/74). EB acknowledges the fellowship with the EU project no. POWR.03.02.00-00-I013/16. The open-access publication of this article was funded by the Priority Research Area BioS under the program "Excellence Initiative – Research University" at the Jagiellonian University in Krakow.

Authors would like to address special thanks to Ms. Renata Budzynska (JCET UJ) for cell culture maintenance.

References

[1] W.C. Aird, Endothelium in health and disease, Pharmacol. Rep. 60 (2008) 139–143.
[2] A. Daiber, S. Chlopicki, Revisiting pharmacology of oxidative stress and endothelial dysfunction in cardiovascular disease: evidence for redox-based therapies, Free Radic. Biol. Med. (2020) 1–23.
[3] J.Y. Lee, O.N. Bae, S.M. Chung, M.Y. Lee, J.H. Chung, Menadione induces endothelial dysfunction mediated by oxidative stress and arylation, Chem. Biol. Interact. 137 (2001) 169–183.
[4] C.L. Kao, L.K. Chen, Y.L. Chang, M.C. Yung, C.C. Hsu, Y.C. Chen, W.L. Lo, S. J. Chen, H.H. Ku, S.J. Hwang, Resveratrol protects human endothelium from H2O2-induced oxidative stress and senescence via SirT1 activation, J. Atheroscler. Thromb. 17 (2010) 970–979.
[5] R. Kohen, A. Nyska, Invited review: oxidation of biological systems: oxidative stress phenomena, antioxidants, redox reactions, and methods for their quantification, Toxicol. Pathol. 30 (2002) 620–650.
[6] Y. Higashi, K. Noma, M. Yoshizumi, Y. Kihara, Endothelial function and oxidative stress in cardiovascular diseases, Circ. J. 73 (2009) 411–418.
[7] M. Redza-Dutordoir, D.A. Averill-Bates, Activation of apoptosis signalling pathways by reactive oxygen species, Biochim. Biophys. Acta, Mol. Cell Res. 1863 (2016) 2977–2992.
[8] N.D. Vaziri, B. Rodríguez-Iturbe, Mechanisms of disease: oxidative stress and inflammation in the pathogenesis of hypertension, Nat. Clin. Pract. Nephrol. 2 (2006) 582–593.
[9] D.G. Harrison, J. Widder, I. Grumbach, W. Chen, M. Weber, C. Searles, Endothelial mechanotransduction, nitric oxide and vascular inflammation, J. Intern. Med. 259 (2006) 351–363.
[10] J. Li, X. Zuo, P. Cheng, X. Ren, S. Sun, J. Xu, A. Holmgren, J. Lu, The production of reactive oxygen species enhanced with the reduction of menadione by active thioredoxin reductase, Metallomics 11 (2019) 1490–1497.
[11] W.C. McAmis, R.C. Schaeffer, J.W. Baynes, M.B. Wolf, Menadione causes endothelial barrier failure by a direct effect on intracellular thiols, independent of reactive oxidant production, Biochim. Biophys. Acta, Mol. Cell Res. 1641 (2003) 43–53.
[12] J.M. May, Z.C. Qu, X. Li, Ascorbic acid blunts oxidant stress due to menadione in endothelial cells, Arch. Biochem. Biophys. 411 (2003) 136–144.
[13] M.C. Warren, E.A. Bump, D. Medeiros, S.J. Braunhut, Oxidative stress-induced apoptosis of endothelial cells, Free Radic. Biol. Med. 29 (2000) 537–547.
[14] D. Jawniak, R. Jawniak, M. Małek, M. Górska, Wpływ stresu oksydacyjnego na przebieg kliniczny ostrych białaczek mieloblastycznych, Reports Pract. Oncol. Radiother. 9 (2004) 157–160.
[15] S.M. Bailey, A. Landar, V. Darley-Usmar, Mitochondrial proteomics in free radical research, Free Radic. Biol. Med. 38 (2005) 175–188.
[16] P. Pagsberg, R. Wilbrandt, K.B. Hansen, K.V. Weisberg, Fast resonance raman spectroscopy of short-lived radicals, Chem. Phys. Lett. 39 (1976) 538–541.
[17] T. Morimoto, L. Da Chiu, H. Kanda, H. Kawagoe, T. Ozawa, M. Nakamura, K. Nishida, K. Fujita, T. Fujikado, Using redox-sensitive mitochondrial cytochrome Raman bands for label-free detection of mitochondrial dysfunction, Analyst 144 (2019) 2531–2540.
[18] V. Sriramoju, A. Alimova, R. Chakraverty, A. Katz, S.K. Gayen, L. Larsson, H. E. Savage, R.R. Alfano, Raman spectroscopic study of acute oxidative stress induced changes in mice skeletal muscles, Biomed. Opt. Spectrosc. 6853 (2008) 685315.
[19] J. Noonan, S.M. Asiala, G. Grassia, N. MacRitchie, K. Gracie, J. Carson, M. Moores, M. Girolami, A.C. Bradshaw, T.J. Guzik, G.R. Meehan, H.E. Scales, J.M. Brewer, I. B. McInnes, N. Sattar, K. Faulds, P. Garside, D. Graham, P. Maffia, In vivo multiplex molecular imaging of vascular inflammation using surface-enhanced Raman spectroscopy, Theranostics 8 (2018) 6195–6209.
[20] E. Efeoglu, M.A. Maher, A. Casey, H.J. Byrne, Label-free, high content screening using Raman microspectroscopy: the toxicological response of different cell lines to amine-modified polystyrene nanoparticles (PS-NH 2), Analyst 142 (2017) 3500–3513.

[21] E. Brauchle, S. Thude, S.Y. Brucker, K. Schenke-Layland, Cell death stages in single apoptotic and necrotic cells monitored by Raman microspectroscopy, Sci. Rep. 4 (2014) 1–9.
[22] K. Majzner, A. Kaczor, N. Kachamakova-Trojanowska, A. Fedorowicz, S. Chlopicki, M. Baranska, 3D confocal Raman imaging of endothelial cells and vascular wall: perspectives in analytical spectroscopy of biomedical research, Analyst 138 (2013) 603–610.
[23] E. Eruslanov, S. Kusmartsev, Identification of ROS using oxidized DCFDA and flow-cytometry, Methods Mol. Biol. 594 (2010) 57–72.
[24] B. Chazotte, Labeling mitochondria with mitotracker dyes, Cold Spring Harb Protoc 6 (2011) 990–992.
[25] M.Z. Pacia, M. Sternak, L. Mateuszuk, M. Stojak, A. Kaczor, S. Chlopicki, Heterogeneity of chemical composition of lipid droplets in endothelial inflammation and apoptosis, Biochim. Biophys. Acta, Mol. Cell Res. 2020 (1867) 118681.
[26] E. Matuszyk, E. Sierka, M. Rodewald, H. Bae, T. Meyer, E. Kus, S. Chlopicki, M. Schmitt, J. Popp, M. Baranska, Differential response of liver sinusoidal endothelial cells and hepatocytes to oleic and palmitic acid revealed by Raman and CARS imaging, Biochim. Biophys. Acta Mol. basis Dis. 2020 (1866) 165763.
[27] K. Majzner, K. Kochan, N. Kachamakova-Trojanowska, E. Maslak, S. Chlopicki, M. Baranska, Raman imaging providing insights into chemical composition of lipid droplets of different size and origin: in hepatocytes and endothelium, Anal. Chem. 86 (2014) 6666–6674.
[28] A. Rygula, K. Majzner, K.M. Marzec, A. Kaczor, M. Pilarczyk, M. Baranska, Raman spectroscopy of proteins: a review, J. Raman Spectrosc. 44 (2013) 1061–1076.
[29] F.M. Lyng, I.R.M. Ramos, O. Ibrahim, H.J. Byrne, Vibrational microspectroscopy for cancer screening, Appl. Sci. 5 (2015) 23–35.
[30] K. Czamara, K. Majzner, A. Selmi, M. Baranska, Y. Ozaki, A. Kaczor, Unsaturated lipid bodies as a hallmark of inflammation studied by Raman 2D and 3D microscopy, Sci. Rep. 7 (2017) 1–10.
[31] Z. Hong, S.A. Asher, Dependence of Raman and resonance Raman intensities on sample self-absorption, Appl. Spectrosc. 69 (2015) 75–83.
[32] K. Czamara, K. Majzner, M. Pilarczyk, K. Kochan, A. Kaczor, M. Baranska, K. Czamara, K. Majzner, M.Z.Z. Pacia, K. Kochan, A. Kaczor, M. Baranska, Raman spectroscopy of lipids: a review, J. Raman Spectrosc. 46 (2015) 4–20.
[33] M. Köhler, S. MacHill, R. Salzer, C. Krafft, Characterization of lipid extracts from brain tissue and tumors using Raman spectroscopy and mass spectrometry, Anal. Bioanal. Chem. 393 (2009) 1513–1520.
[34] C. Krafft, S.B. Sobottka, G. Schackert, R. Salzer, Raman and infrared spectroscopic mapping of human primary intracranial tumors: a comparative study, J. Raman Spectrosc. 37 (2006) 367–375.
[35] F.A. Miller, H.R. Golob, The infrared and Raman spectra of cyclohexane and cyclohexane-d12, Spectrochim. Acta 20 (1964) 1517–1530.
[36] G. Socrates, Infrared and Raman Characteristic Group Frequencies Tables and Charts, John Wiley & Sons, LTD Chichester, 2001.
[37] R.N.J.K. Noack, Some Streochemica, Studies on α,β-Unsaturated Ketones Using Raman Spectrophometry 39, 1961.
[38] E. Bik, A. Dorosz, L. Mateuszuk, M. Baranska, K. Majzner, Fixed versus live endothelial cells: the effect of glutaraldehyde fixation manifested by characteristic bands on the Raman spectra of cells, Spectrochim. Acta - Part A Mol. Biomol. Spectrosc. 240 (2020) 118460.
[39] B. Hernández, F. Pflüger, S.G. Kruglik, M. Ghomi, Characteristic Raman lines of phenylalanine analyzed by a multiconformational approach, J. Raman Spectrosc. 44 (2013) 827–833.
[40] R.G. Kranz, C. Richard-Fogal, J.-S. Taylor, E.R. Frawley, Cytochrome c biogenesis: mechanisms for covalent modifications and trafficking of heme and for heme-iron redox control, Microbiol. Mol. Biol. Rev. 73 (2009) 510–528.
[41] M. Kakita, V. Kaliaperumal, H.O. Hamaguchi, Resonance Raman quantification of the redox state of cytochromes b and c in-vivo and in-vitro, J. Biophotonics 5 (2012) 20–24.
[42] J.F. Hsu, P.Y. Hsieh, H.Y. Hsu, S. Shigeto, When cells divide: Label-free multimodal spectral imaging for exploratory molecular investigation of living cells during cytokinesis, Sci. Rep. 5 (2015).